NASA TECHNICAL NOTE

NASA TN D-2553

PERFORMANCE OF 84° FLAT-PLATE HELICAL INDUCER AND COMPARISON WITH PERFORMANCE OF SIMILAR 78° AND 80.6° INDUCERS

by Douglas A. Anderson, Richard F. Soltis, and Donald M. Sandercock

Lewis Research Center
Cleveland, Ohio

NATIONAL AERONAUTICS AND SPACE ADMINISTRATION • WASHINGTON, D. C. • DECEMBER 1964

PERFORMANCE OF 84° FLAT-PLATE HELICAL INDUCER AND COMPARISON WITH PERFORMANCE OF SIMILAR 78° AND 80.6° INDUCERS

By Douglas A. Anderson, Richard F. Soltis,
and Donald M. Sandercock

Lewis Research Center
Cleveland, Ohio

NATIONAL AERONAUTICS AND SPACE ADMINISTRATION

For sale by the Office of Technical Services, Department of Commerce,
Washington, D.C. 20230 -- Price $2.00

PERFORMANCE OF 84° FLAT-PLATE HELICAL INDUCER AND COMPARISON WITH PERFORMANCE OF SIMILAR 78° AND 80.6° INDUCERS

by Douglas A. Anderson, Richard F. Soltis, and Donald M. Sandercock

Lewis Research Center

SUMMARY

A flat-plate, constant-lead helical inducer with an 84° tip angle was tested in the Lewis water tunnel. The inducer was tested in cold water over a range of flow rates at various net positive suction heads. Both the overall performance and the radial distributions of flow parameters were observed. The radial distributions describe the type of flow patterns occurring across the rotor and show the radial variation of flow conditions that a succeeding pump stage must accept. The validity of the simple radial equilibrium assumption over a range of flow conditions is verified.

The performance of this 84° helical inducer is compared with the performance of similar inducers with tip helix angles of 78° and 80.6°. A given percentage decrease in performance from the noncavitating level is achieved at decreasing values of cavitation number as the blade tip helix angle is increased. Obtaining lower cavitation numbers through the use of higher helix angle blading, however, does not necessarily mean obtaining increased suction specific speeds.

INTRODUCTION

The cavitating inducer is commonly used to increase the suction specific speed of pumps for missile application and thus to reduce pump weight and size. One type of inducer, the flat-plate helix, was selected as a convenient test vehicle to study cavitation phenomena. While a large amount of information on the helical inducer exists, most investigations are directed toward measurements of overall performance that were supplemented by photographs and visual observations of cavitation phenomena.

In this study, several typical inducers were selected and radial distributions of pressure and velocity at the rotor inlet and outlet were obtained in addition to overall performance and visual observations. These data provide further insight into the flow through the inducer and the limitations on its

operating range; the radial distribution of velocity diagrams and pressures that a succeeding blade row must accept are also shown. References 1 and 2 report performance details for helical inducers with tip angles of 78° and 80.6°, respectively.

This report presents the overall and detailed performance for a range of inlet pressures of a flat-plate helical inducer of constant lead with an 84° blade angle at the tip. The overall performance results of the 84° helix angle inducer reported herein combined with the results of references 1 and 2 cover a significant portion of the practical range of inducer operation. Trends of cavitation similarity parameters with helix angle for inducers with this type blading are indicated.

APPARATUS AND PROCEDURE

The test rotor was a three-bladed, constant-lead, helical inducer with a tip angle of 84° (defined as the angle between the blade meanline and the axial direction). It had a constant tip diameter of 4.986 inches and a hub-to-tip ratio of approximately 0.5. The detailed geometric features of the rotor are presented in table I. A photograph of the rotor is shown in figure 1.

The rotor was machined from 400 series stainless steel. Both leading and trailing edges were sharpened to a wedge shape symmetrical about the blade centerline.

The investigation was conducted in the Lewis water tunnel, which is shown in figure 2. Since the test facility, apparatus, and procedures that were used are identical to those given in reference 1, they will not be discussed in detail in this report. The test fluid was 80° F water with an air content of less than 3 parts per million by weight. Figure 3 is a photograph of the test section and associated

TABLE I. - GEOMETRY OF 84° HELICAL INDUCER

Rotor tip diameter (constant), in.	4.986
Rotor hub diameter (constant), in.	2.478
Hub-tip ratio	0.497
Number of blades	3
Axial length, in.	1.637
Peripheral extent of each blade, deg	360
Radial tip clearance, in.	0.025
Tip clearance ratio, tip clearance/blade height	0.020
Tip chord length, in.	15.75
Hub chord length, in.	7.955
Solidity at tip	3.016
Solidity at hub	3.066
Blade tip thickness, in.	0.067
	Linear variation
Blade hub thickness, in.	0.100
Length of tip leading edge wedge fairing, in.	1.00
Length of hub leading edge wedge fairing, in.	1.50

Figure 1. - Helical inducer with 84° tip angle.

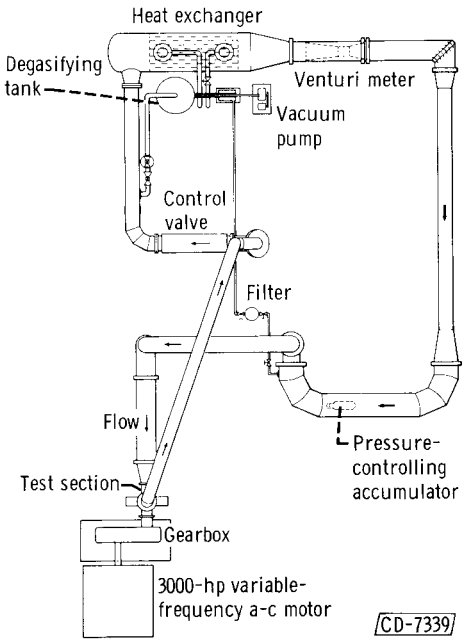

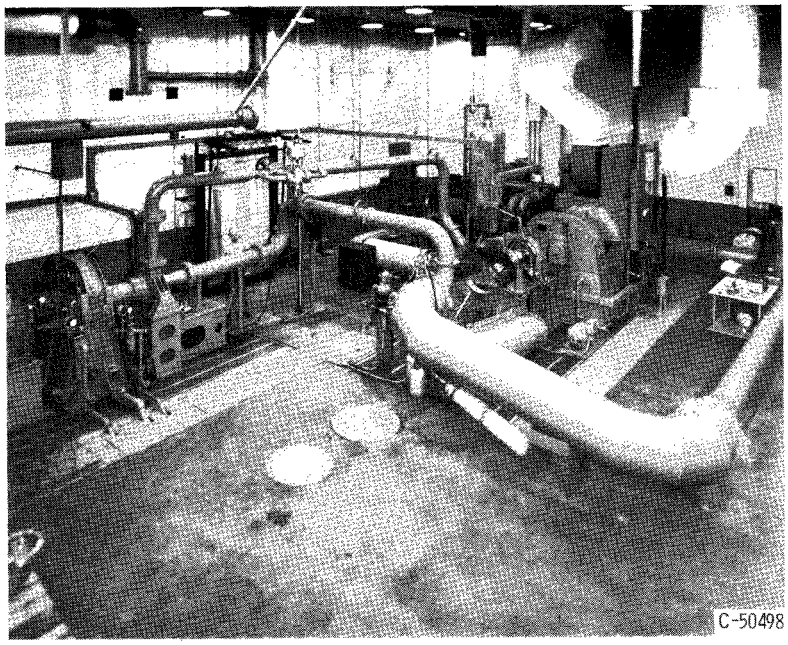

Figure 2. - Test facility.

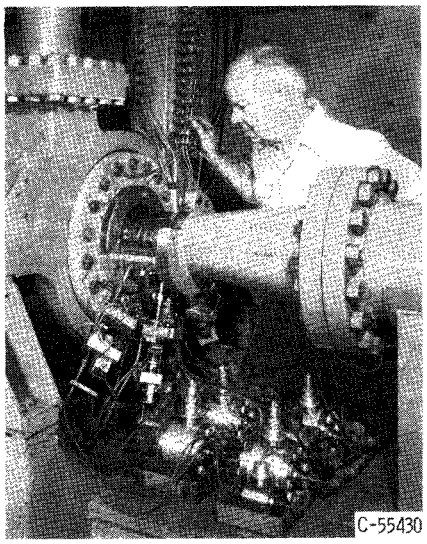

Figure 3. - Rotor test section and location of instrumentation.

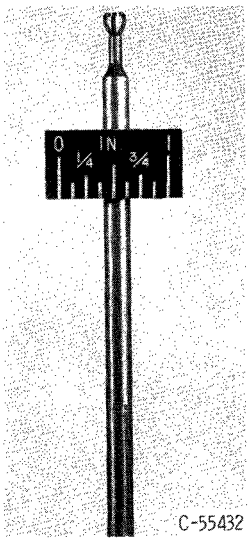

(a) Total-pressure claw.

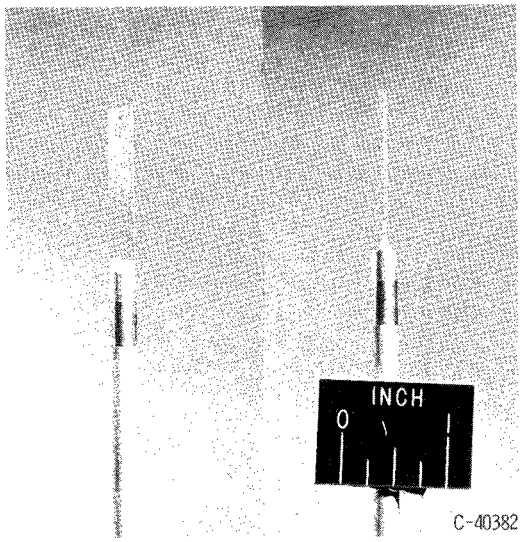

(b) Static-pressure wedge.

Figure 4. - Probes.

instrumentation. Total pressures, static pressures, and fluid angles were measured at seven radial positions, approximately 1 inch upstream of the rotor inlet and 1 inch downstream of the rotor exit. Photographs of the total-pressure and yaw probe and the static-pressure probe are shown in figures 4(a) and (b), respectively. Calibration of the static-pressure probes and setting of the zero angles on both types of probes were accomplished in a low-speed air tunnel. Flow rate was calculated from pressure measurements across a Venturi flowmeter. All data were recorded by using transducers and an automatic digital potentiometer.

TABLE II. - ESTIMATED MAXIMUM INSTRUMENTATION ERRORS

	Error	Operating range
Inlet total pressure, lb/sq in. gage	0.1	-20 to 20
Inlet dynamic velocity head, lb/sq in.	0.25	0 to 50
Head rise across inducer, lb/sq in.	1.5	0 to 300
Outlet dynamic velocity head, lb/sq in.	0.25	0 to 50
Fluid angle, deg	0.5	-20 to 120
Venturi flow reading, percent	2 to 4	
Rotor speed, percent	0.2	
Radial position of probes	1 percent of passage height	

All tests were conducted at a rotative speed of 10,000 rpm. Data points were selected to cover the complete flow range at four inlet pressures. The limits were set by the open throttle position, and at low flows by pressure fluctuations that lead to excessive system vibrations.

In addition to the performance data, photographs of the impeller operating with cavitation were taken on 70-millimeter film in conjunction with a very short duration flash, which stopped the motion of the blades. The different forms and degrees of cavitation within the rotor were observed at the various inducer operating points.

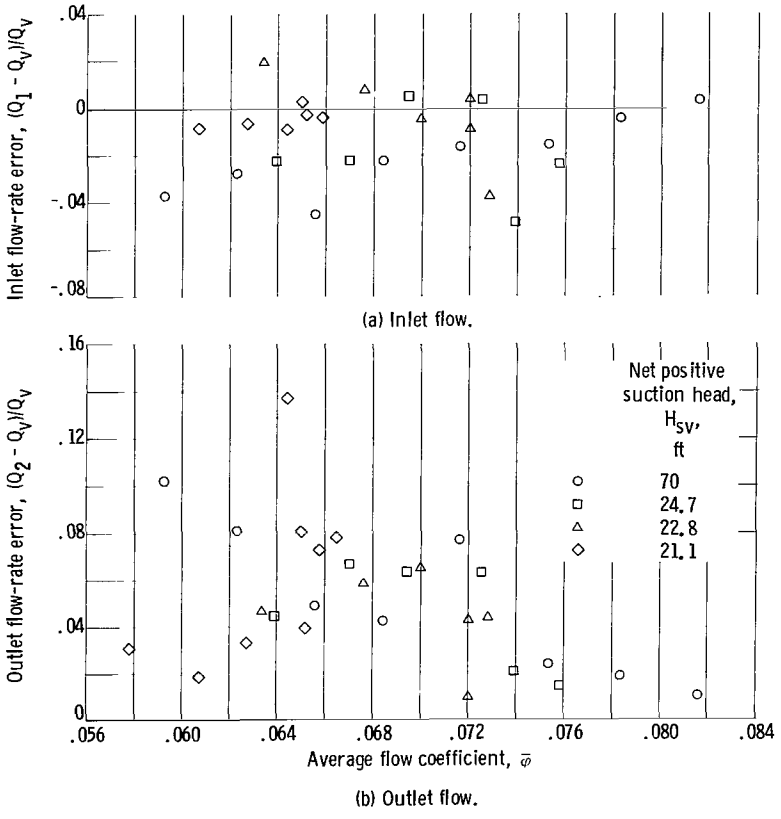

Figure 5. - Comparison of integrated flow with flow measured by Venturi meter.

The estimated maximum measurement errors due to instrumentation are summarized in table II. These errors are inherent in the measuring devices and do not include the effects on the response of the measuring devices due to adverse flow conditions, such as reverse-flow regions, unsteady operation, circumferential and/or radial velocity gradients, and cavitation on the probes.

Figures 5(a) and (b) present a comparison between the integrated weight flow at the rotor-inlet and rotor-outlet measuring stations and the flow measured by the Venturi meter. Thus they serve as a check on the reliability of the velocity diagram data used to calculate the inducer performance param-

eters. At the rotor inlet the integrated flows agree quite favorably with the measured Venturi flows, most comparisons being within 3 percent. The agreement at the outlet measuring station is also reasonably good, most comparisons being within 8 percent. It should be noted that the integrated weight flow is always greater than the measured flow at this outlet station.

The equations defining the parameters used to describe the inducer performance are presented in appendix B. (Symbols are defined in appendix A). The blade-element parameters, calculated from probe measurements at seven selected radial positions, give a complete description of the flow field as it varies with radius. The overall parameters are obtained by an integration of the flow conditions over the entire flow annulus. Reference 2 gives a detailed discussion of the parameters used. In all cases axisymmetric flow is assumed.

RESULTS AND DISCUSSION

The initial step in an investigation of this type is to determine the minimum inlet pressure at which the measured performance is not affected by cavitation. Operation above and below this pressure is then defined as noncavitating and cavitating, respectively.

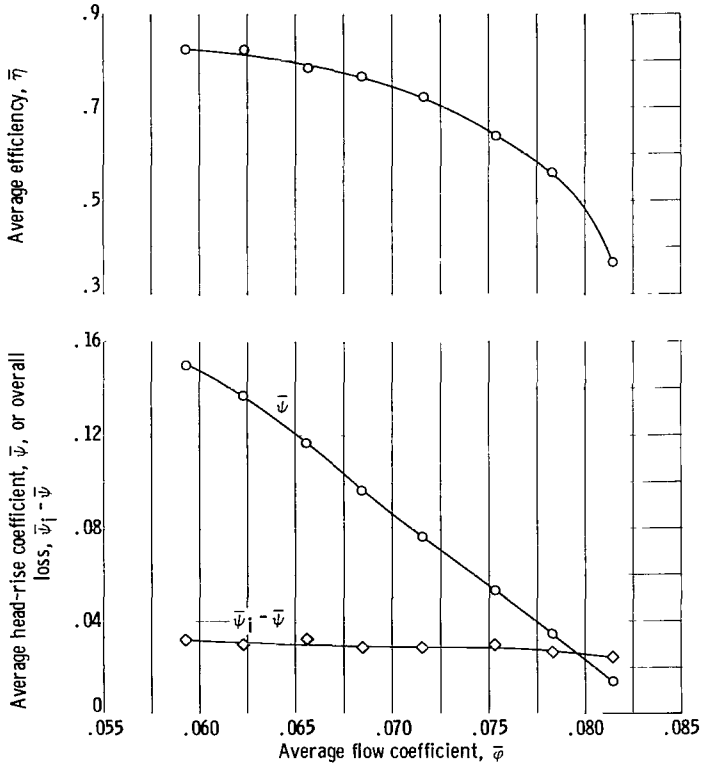

Figure 6. - Overall noncavitating performance. Net positive suction head, 70 feet.

Noncavitating performance

For this investigation 70 feet was selected as the net positive suction head (H_{SV}) at which to obtain noncavitating performance. This value is well above the level at which the first effects of reduced inlet pressure on measured performance were noted. At the rotor speed and H_{SV} that were used, the cavitation number $\bar{k}$ was approximately 0.09. Photographs of the flow at this pressure showed that there was some cavitation occurring both in the tip vortex and on the blade surface. (The designation noncavitating is meant to refer only to measured performance.)

Overall performance. The overall (mass-averaged) performance of the inducer under noncavitating conditions is presented in figure 6. The plot of head coefficient against flow

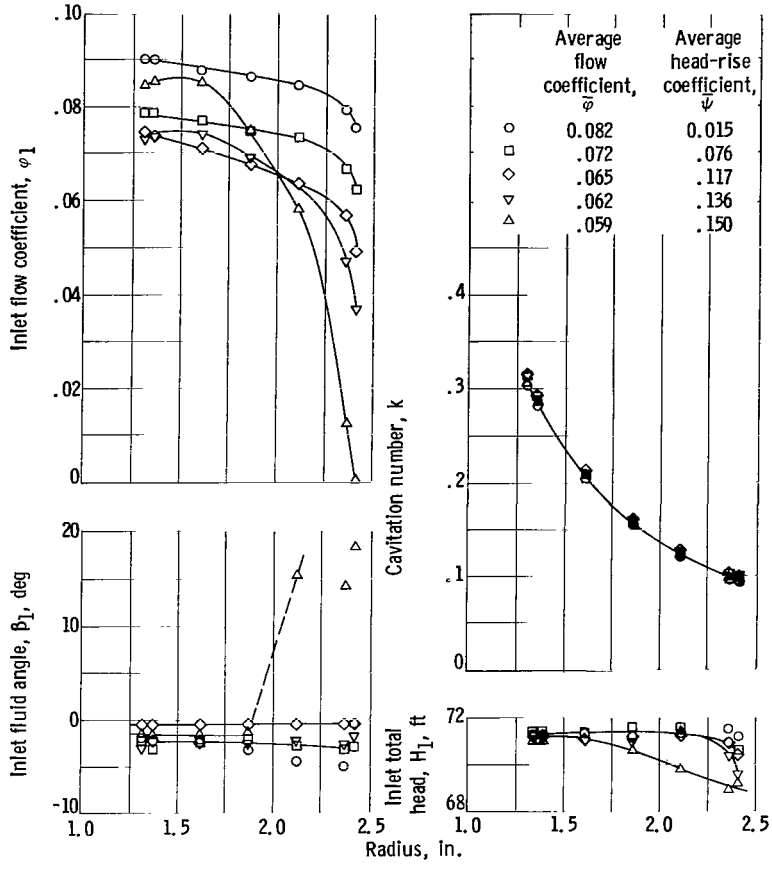

Figure 7. - Radial distribution of inlet flow parameters. Net positive suction head, 70 feet.

coefficient is typical for axial flow inducers. The efficiency (eq. (B18)) has a maximum value of 82.6 percent at the lowest flow coefficient (φ = 0.059) and consistently decreases in value as the flow coefficient is increased. The quantity $\bar{\psi}_i - \bar{\psi}$ is included as a measure of the overall losses. As the losses tend to decrease slightly as flow coefficient is increased, the large changes in efficiency with flow coefficient must be due to changes in energy addition.

Inlet conditions. - Figure 7 shows the radial variations of selected inlet parameters at five flow rates that cover the range of noncavitating operation: (1) flow coefficient φ_1, (2) cavitation number k, (3) total head H_1, and (4) fluid angle β_1. From maximum flow (φ = 0.082) to a flow coefficient of about 0.065, the radial distributions of flow display similar gradients of inlet flow coefficient, the level reflecting the change in flow. Below an average flow coefficient of 0.065 the radial gradient of flow coefficient begins to increase, and as flow is further reduced, the gradient increases very rapidly, the flow coefficient in the tip region going to zero. This latter condition indicates the formation of a reverse-flow region, or eddy, at the tip. Two factors that may contribute to this eddy formation are

(1) Streamline curvature through the rotor with its attendant equilibrium requirements; accompanying the eddy formation in the inlet tip region are similar eddy formations on the hub region at the blade outlet; flow shifts result in streamlines curving away from the hub

(2) Blade tip clearance flows that combine with the through flows to form a vortex, whose extent and location is made visible through cavitation in the vortex core

Thus, at least two contributing factors for the eddy formation can be identified. Data obtained in and close to a reverse flow region generally prove unreliable, and care must be exercised in any interpretation.

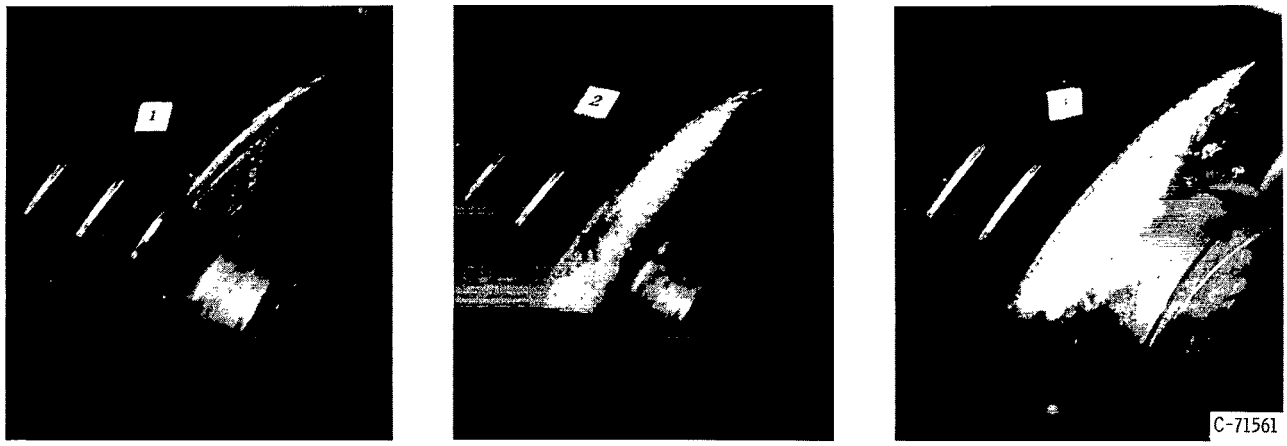

Average flow coefficient	0.81	0.071	0.062
Average head-rise coefficient	0.015	0.077	0.136

Figure 8. - Flow at high net positive suction head. Tip vortex increases as flow coefficient decreases.

Both inlet total head and absolute fluid angles remain essentially constant across the passage (except for a slight influence of outer-casing boundary layer on the total head) until the eddy region occurs.

The location of the tip vortex at three flow coefficients can be observed in figure 8. Although these photographs are taken at the noncavitating H_{SV} of 70 feet, enough cavitation is present to make the tip vortex visible. (The designation noncavitating merely means that this small amount of cavitation does not affect the measured performance.) Values of average flow coefficient $\bar{\varphi}$, average head-rise coefficient $\bar{\psi}$, and net positive suction head H_{SV} are included on these and subsequent photographs to relate observations on these photographs to measured performance levels and location on the overall performance map. In general, maintaining a constant net positive suction head while flow is varied from the open throttle position to some lower value of flow (direction of increased blade loading) results in increased cavitation in the tip vortex region. Thus, figure 8 shows the cavitating tip vortex enlarging and moving increasing distances away from the blade surface and into the inlet passage as the flow coefficient is decreased.

Outlet conditions. - Figure 9 presents the radial distributions of the outlet parameters at the same flow rates at which the inlet parameters were presented. The trends observed here are similar to those observed in references 1 and 2 for 78° and 80.6° inducers; hence, the ensuing discussion may be regarded as applying to the flat-plate helical inducer in general.

Inherently, the flat-plate inducer transmits a radial gradient of energy addition (ψ_i) to the fluid. This can be demonstrated by calculating radial gradients of energy addition and the outlet flow coefficient with assumptions of perfect guidance by the blades and no losses (ref. 3). In real flow, of course, the energy addition is affected by deviation angle, blade flow losses, and axial velocity.

Figure 9 shows that over the upper half of the blade height the gradient

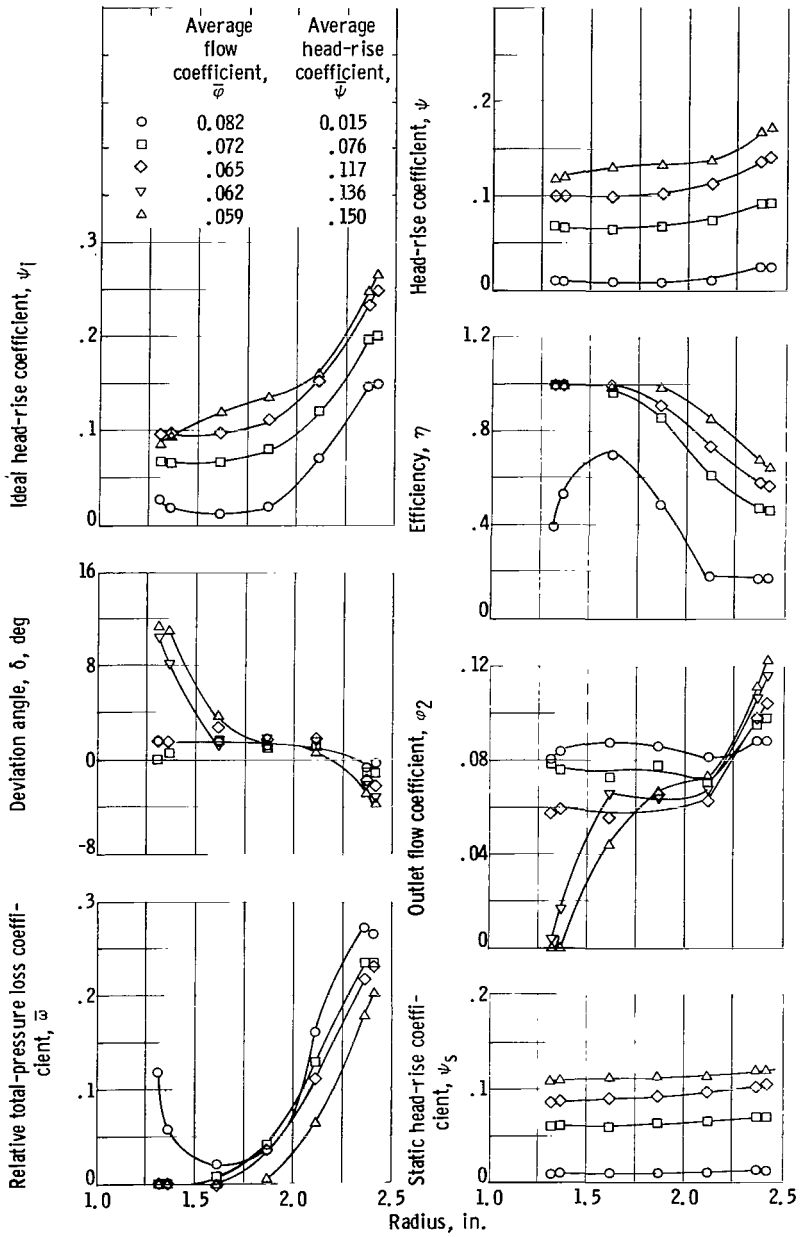

Figure 9. - Radial distribution of outlet flow parameters. Net positive suction head, 70 feet.

of energy addition is very steep, while from the hub to the mean blade height the gradients are relatively small. The gradients over this latter portion of the blade height more closely approximate the gradients obtained from perfect guidance, no-loss calculations.

In any interpretation of the deviation angle results shown herein, it should be kept in mind that the indicated deviation angles, taken from measurements 1 inch downstream of the blade trailing edge, may differ from the true deviation angles occurring at the trailing edge. In normal compressor practice, the difference is neglected, but a considerable difference can result from large radial flows occurring between the trailing edge and the outlet measuring station. This condition is typical for inducer operation at all but the highest flow coefficients.

The indicated deviation angles, in general, decrease in value from hub to tip, negative values being computed in the tip regions. Similar results were reported in references 1 and 2 for 78° and 80.6° flat-plate helical inducers. Reference 1 presents a simple calculation that relates the velocity diagram existing at the trailing edge to the measured velocity diagram if the change in streamline radius between the trailing edge and the measuring station is known. Because this cannot be determined from the measured data, the calculation gives only an estimate of the true deviation angle. The calculation shows, however, that relatively small changes in radius for the streamlines in the tip region would result in differences between the true deviation angles

and the indicated angles large enough to eliminate the negative values. Of course, the influence of some other flow phenomenon, for instance, the effects of the outer casing walls on this type of flow, cannot be entirely eliminated.

The radial distribution of loss coefficient $\bar{\omega}$ in figure 9 shows that, in general, the trends were similar at all flows, a relatively low or zero value at the hub increasing slightly to the midpassage region and then increasing sharply from the midpassage to the tip region. Analysis of the flow losses across the helical inducer has proven very complicated and must await a better understanding of other flow phenomena, for instance, secondary flow. At present, the following comments can be made:

(1) The trend of loss coefficient with radius noted previously is similar to that observed for helical bladed inducers with different helix angles (refs. 1 and 2).

(2) The extremely low value of loss measured in the hub region and the steep gradient of loss from midspan to the tip region are interpreted as an indication of the importance of secondary flow losses, radial transport of blade-surface boundary layer, tip-clearance flow losses, etc. in this type of pump rotor.

The radial distributions of axial velocity reflect the requirements of radial equilibrium and continuity. The general trend is for an increasing axial velocity with radius and an increasing gradient as flow is reduced. A flow is finally reached where the axial velocity at the hub is reduced to zero and a reverse-flow region, or eddy, is formed. At a further reduction in flow, excessive pressure fluctuations, originating in the rotor and evidenced as rig vibrations, are encountered.

The measured head-rise coefficient, resulting from the energy addition and loss, increases from hub to tip at all flows. As flow is reduced, the gradient is increased. This trend is typical for helical inducers and is noted in similar tests reported in references 1 and 2.

A static head-rise coefficient ψ_s is included among the blade element parameters because the addition of static pressure is the basic function of the inducer. This additional static-pressure head is needed to suppress cavitation in blade rows behind the inducer. The static head-rise distributions follow the trends of the total head rise but with smaller variations from hub to tip.

The radial variations of efficiency are, in general, the inverse of the loss variations with sharp decreases from the midpassage to the tip region. The change of efficiency for the different flows reflects the effects of both losses and energy input.

From figures 6 and 9, for this 84° inducer only, there is an apparent discrepancy between the overall loss coefficient $\bar{\psi}_i - \bar{\psi}$, which increases slightly as the overall flow coefficient decreases, and the blade-element loss coefficients $\bar{\omega}$, which decrease at all radii when the overall flow coefficient is decreased. At the low flows, a greater part of the flow is in the high-loss tip region, so that the mass average of loss coefficient can increase even though

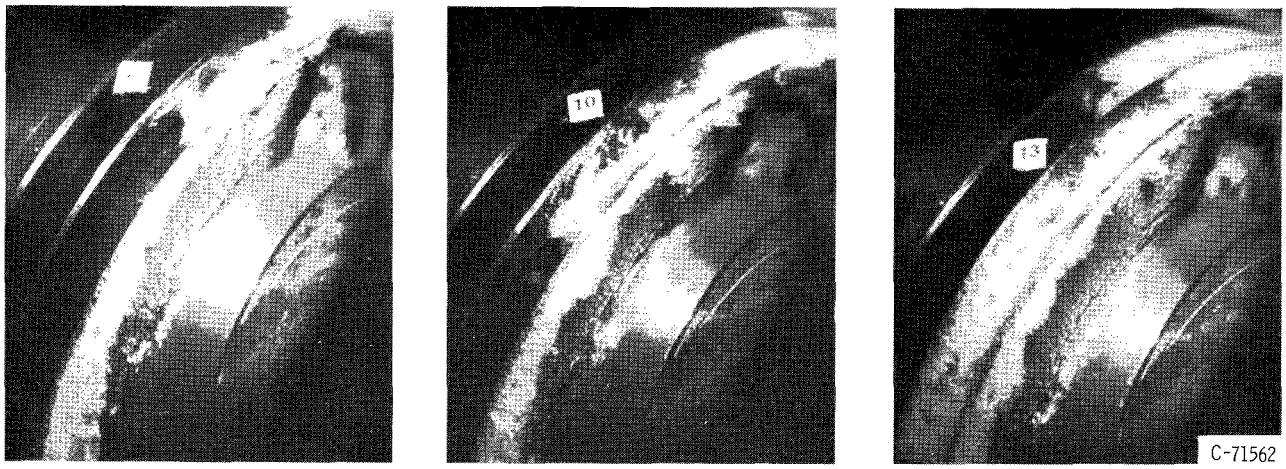

Net positive suction head, ft	24.7	22.8	21.1
Average head-rise coefficient	0.113	0.108	0.095

Figure 10. - Flow at same average flow coefficient (0.064) and varying net positive suction heads.

the individual values of loss coefficient decrease.

Cavitation Performance

To test the effects of cavitation on the measured performance, three inlet pressures were selected at which the inducer performance was measured over a range of flow coefficients. These inlet pressures cover the normal operating range of the inducer, in which a considerable dropoff of the head-rise coefficient from its noncavitating value has taken place.

Photographs of the cavitation at the three inlet pressures are shown in figure 10. They depict the growth of cavitation as H_{SV} is reduced while inlet flow geometry is maintained (approximately the same inlet flow coefficient). In general, it has been shown that the pump-inducer head rise begins to fall off when the blade-surface cavitation extends past the leading edge of the adjacent blade. At the inlet flow coefficient of 0.064, the noncavitating head-rise coefficient is 0.125; thus, some decrease in head rise has occurred at all H_{SV} values shown. The photographs show that, at all H_{SV} values, both blade-surface and tip-vortex cavitation are occurring, and both extend increased distances along the blade passage as H_{SV} is lowered. In all cases the tip-vortex cavitation extends past the leading edge of the adjacent blade. The extent of the blade-surface cavitation is usually slightly less than the more clearly visible tip-vortex cavitation.

Overall performance. - The noncavitating characteristics plus the performance curves of the inducer at three inlet pressures in the cavitating regime are presented in figure 11. The performance parameters include mass-averaged values of head-rise coefficient, efficiency, and net positive suction head, along with an average value of flow coefficient based on measured Venturi flow and the blade-row-inlet geometric flow area. The cavitating performance lies in the suction specific speed range of 23,000 to 26,000. For the values of

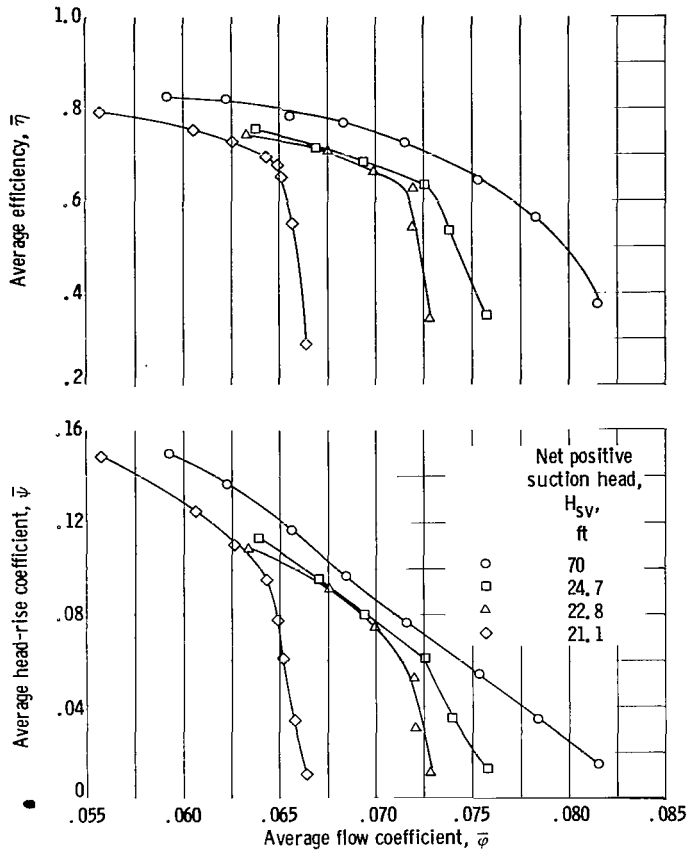

Figure 11. - Overall performance.

H_{sv} of 70.0 and 21.1 feet, the low-flow ends of the curves terminate where excessive pressure fluctuations were encountered. The intermediate H_{sv} curves could have been extended to lower flows, but would have shown small differences in performance from the curves that were run. As usual, breakdown of the head producing capability of the inducer due to cavitation effects occurs first at the highest flow coefficient as inlet pressure (or H_{sv}) is reduced. The nearly vertical portion of the performance characteristic at an H_{sv} of 21.1 feet demonstrates that cavitation limits the flow through the pump.

Another method of presenting cavitating data is in terms of the cavitation number k. Although k, strictly defined, is a function that varies with radius; that is, for $V_{\theta,1} = 0$,

$$k = \frac{h_1 - h_v}{\frac{V_1'^2}{2g}} = \frac{h_1 - h_v}{\frac{U^2 + V_1^2}{2g}} \qquad (1)$$

$\bar{k}$ based on averaged values is often used and is defined as

$$\bar{k} = \frac{2gH_{sv}}{U_t^2(1 + \bar{\varphi}^2)} - \frac{\bar{\varphi}^2}{1 + \bar{\varphi}^2} \qquad (2)$$

Figure 12 shows the mass-averaged head-rise coefficient $\bar{\psi}$ as a function of $\bar{k}$ for constant values of average flow coefficient $\bar{\varphi}$. The data for this type of plot were obtained by interpolating the curves of figure 11. Because of the limited number of values for inlet pressure (H_{sv}) investigated, the curves are not precisely defined; hence, some liberty has been taken in fairing in the lines, particularly in the cavitation inception region (H_{sv} at which cavitation first affects the level of performance). However, the $\bar{k}$ where cavitation breakdown occurred or was imminent (the $\bar{k}$ where a large drop in $\bar{\psi}$ occurred for a small reduction in $\bar{k}$) is reasonably well defined.

In figure 13, where the head coefficient is normalized by dividing by the noncavitating value at the same flow coefficient, all of the test points are plotted, and curves covering a range of flow coefficients are faired. In both figures 12 and 13 the cavitation breakdown point appears to occur at a $\bar{k}$ of

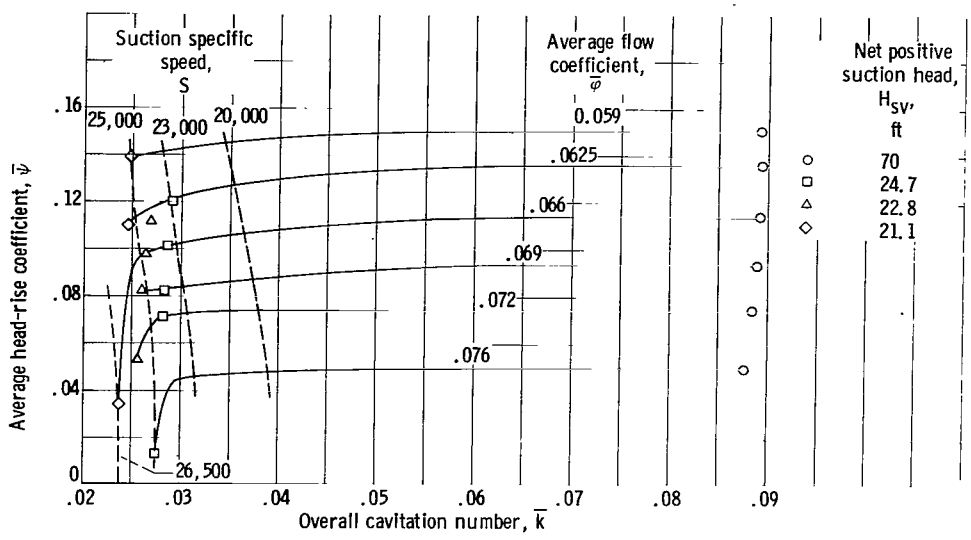

Figure 12. - Inducer performance as function of overall cavitation number.

approximately 0.024, which for a flow coefficient of 0.066 corresponds to a suction specific speed of 26,000.

Radial distributions. - The effects of cavitation on blade element performance are shown in figures 14(a) to (d), which compare the radial distribution of blade element parameters at the same average flow coefficient for different values of cavitation number. Because of the steep slope of the $\bar{\varphi}, \bar{\psi}$ curve (fig. 11), it was necessary to match the flow-coefficient values very closely to produce meaningful comparisons. In most cases, only two H_{sv} values could be matched at the same value of φ for these direct comparisons.

From maximum flow to an inlet average flow coefficient of approximately 0.065 the inlet-flow geometry does not seem to vary with H_{sv} for the range of H_{sv} (or $\bar{k}$) covered in this investigation. Inlet flow angles remain approximately constant across the passage and vary between 0° and -5° over the range of inlet pressure covered. No particular significance is attached to this variation. At the lower inlet pressures, cavitation on the inlet probes may introduce some measurement errors. Apparently no significant prewhirl occurs. The radial variations of flow coefficient indicate that

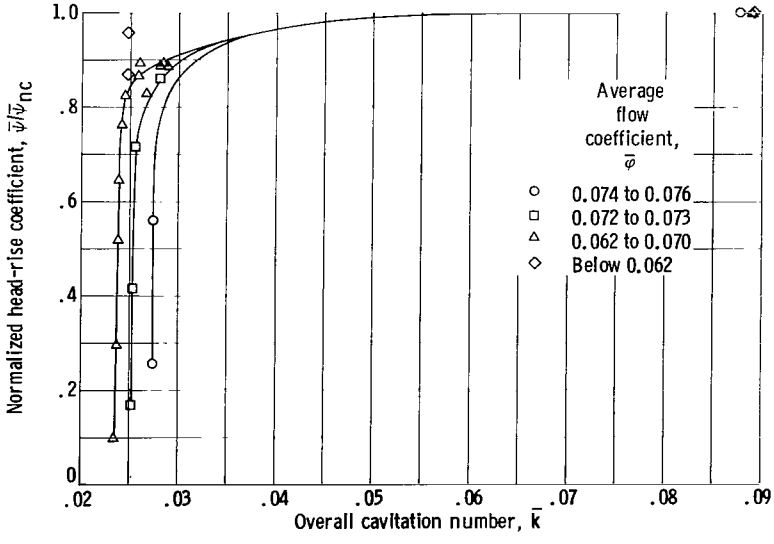

Figure 13. - Composite of cavitation performance.

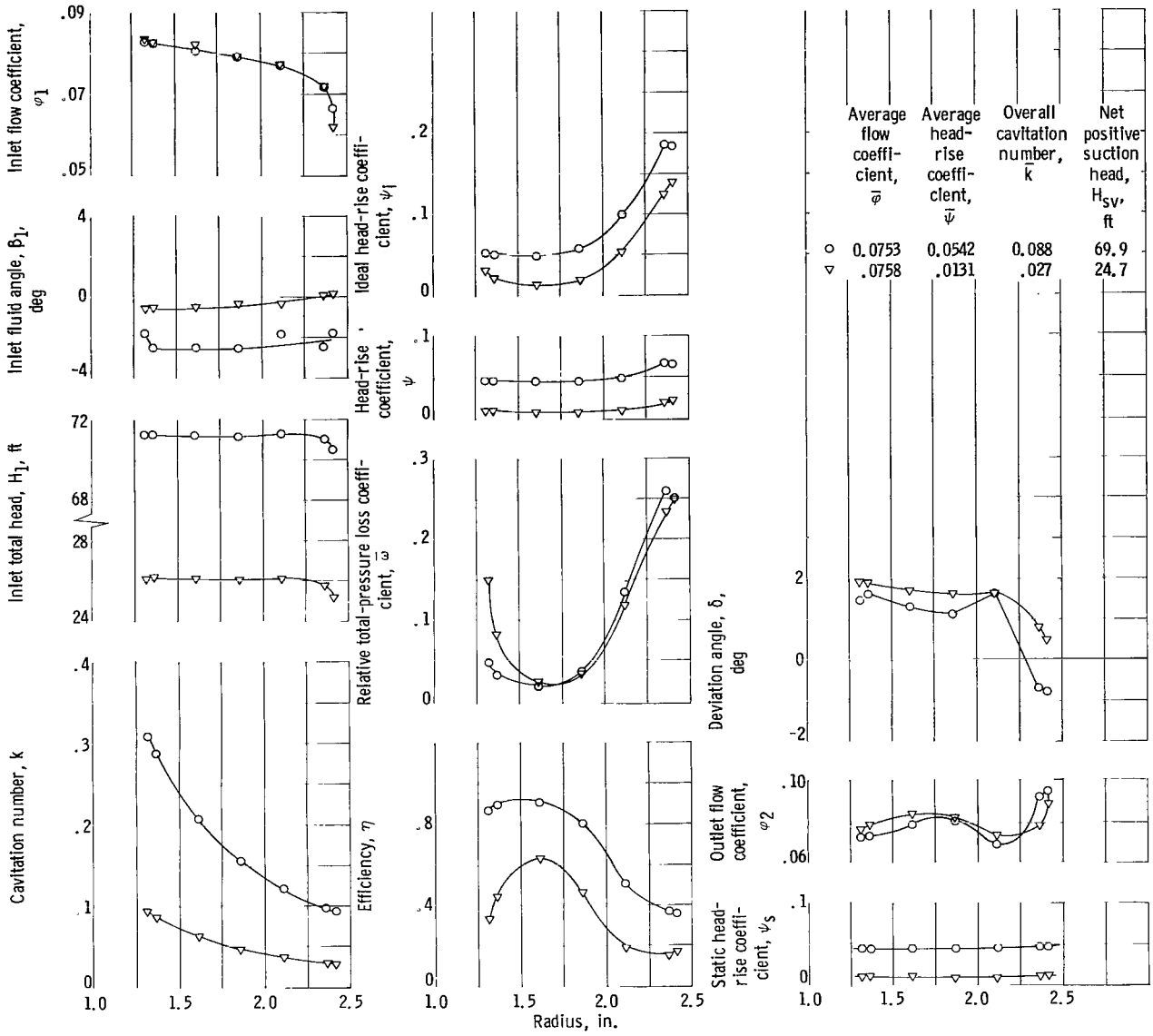

(a) Average flow coefficient, 0.0755.

Figure 14. - Radial distribution of performance parameters.

flow geometry is maintained with the exception of small differences noted in the tip region. In this region, the values are affected by the casing boundary layer, as indicated by the dropoff of inlet total head. In addition, as the inlet pressure is reduced, increased cavitation in the tip vortex may affect the flows in this region. Total pressures are essentially constant across the flow passage with the exception of slight decreases in the tip region, probably due to the casing boundary layer.

As flow is lowered below an average flow coefficient of approximately 0.065, as was noted in the section Noncavitating Performance, the negative

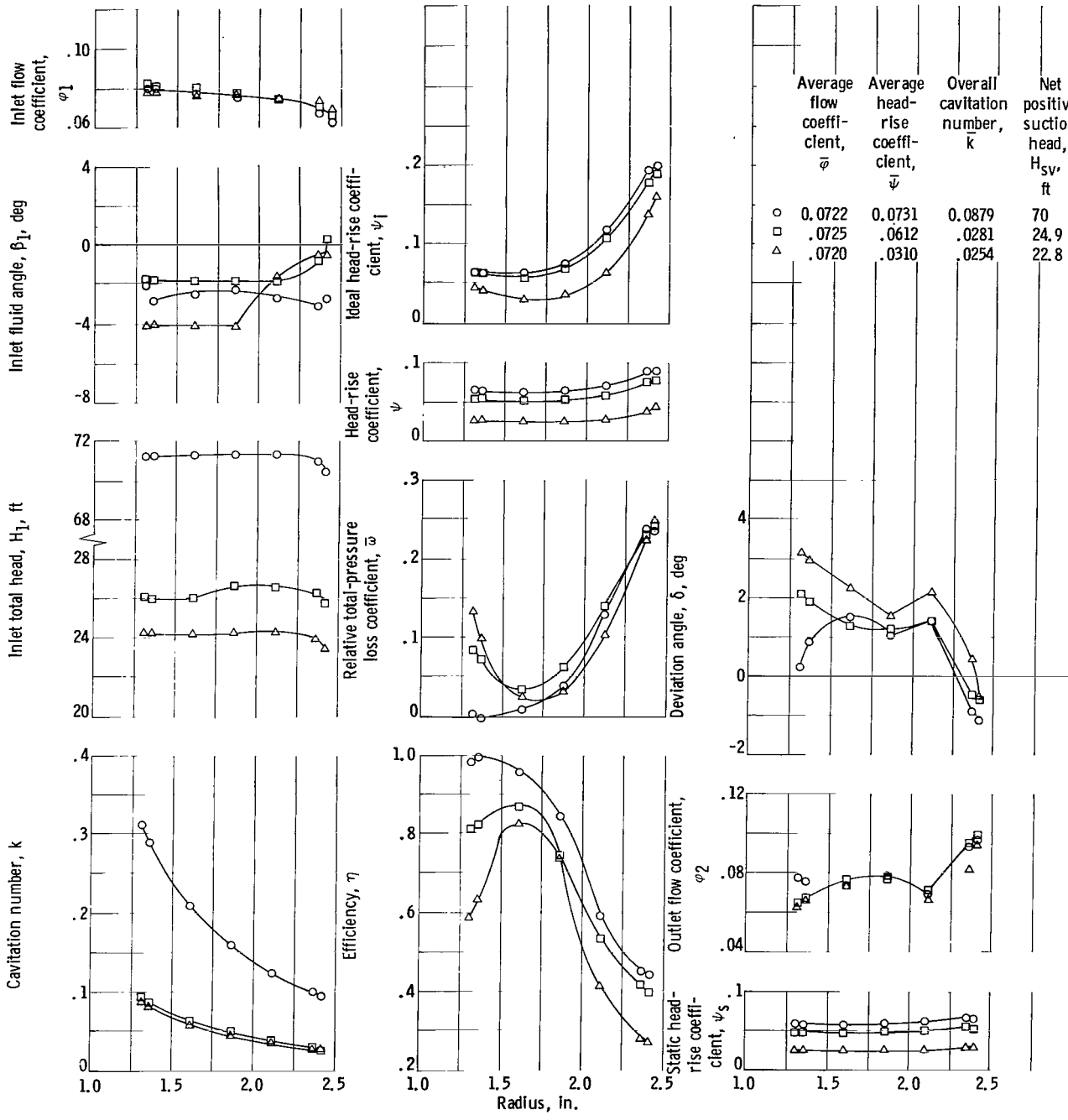

(b) Average flow coefficient, 0.0722.

Figure 14. - Continued. Radial distribution of performance parameters.

radial gradient of inlet flow coefficient with radius increases. The beginning of this trend is shown by the curve for inlet flow coefficient in figure 14(d) for the noncavitating flow condition ($\bar{k}$ = 0.0894). Under cavitating conditions this gradient is reduced and more closely resembles the normal gradient of flow coefficient caused by streamline curvature over the inlet-hub curvature.

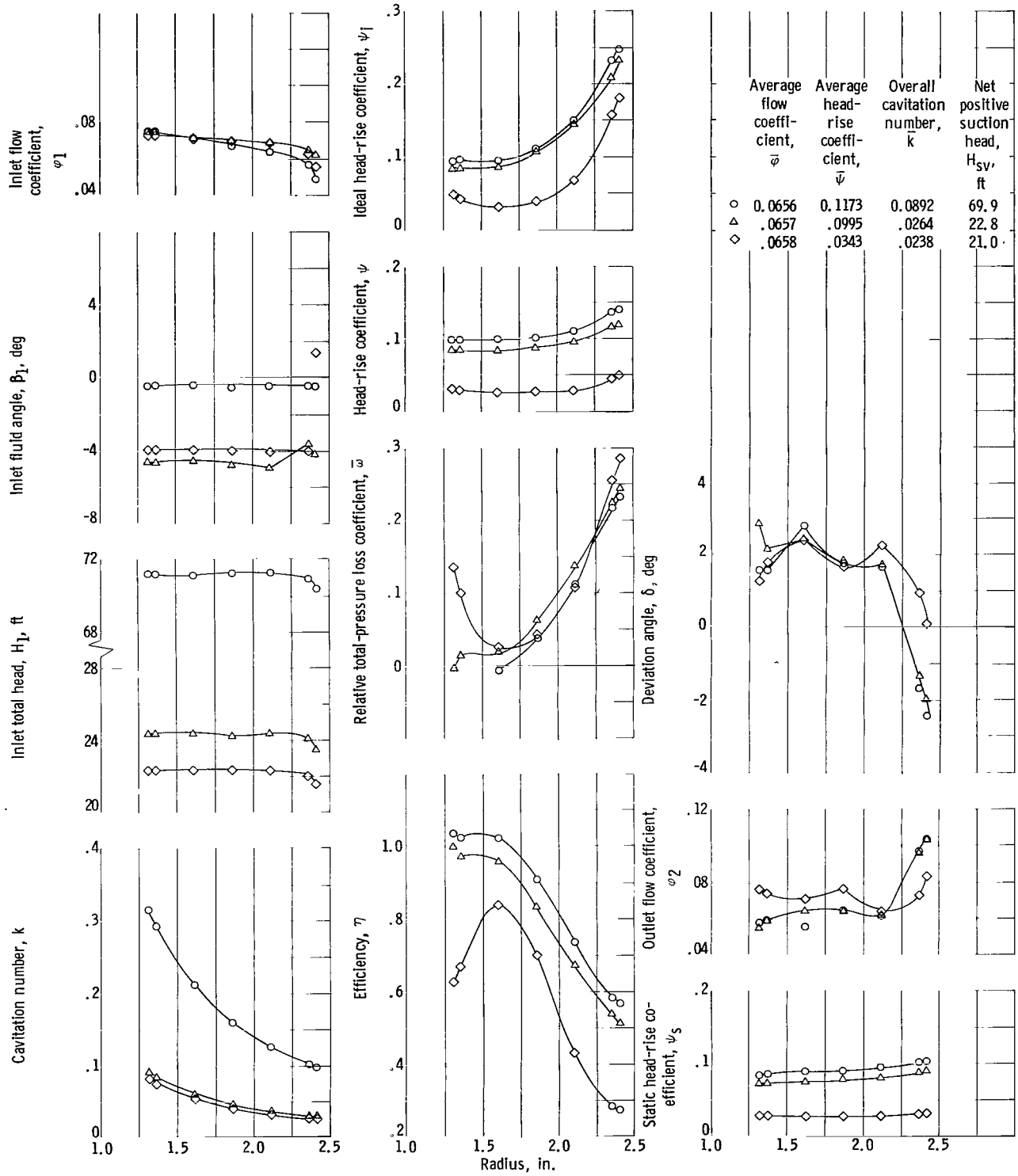

(c) Average flow coefficient, 0.0657.

Figure 14. - Continued. Radial distribution of performance parameters.

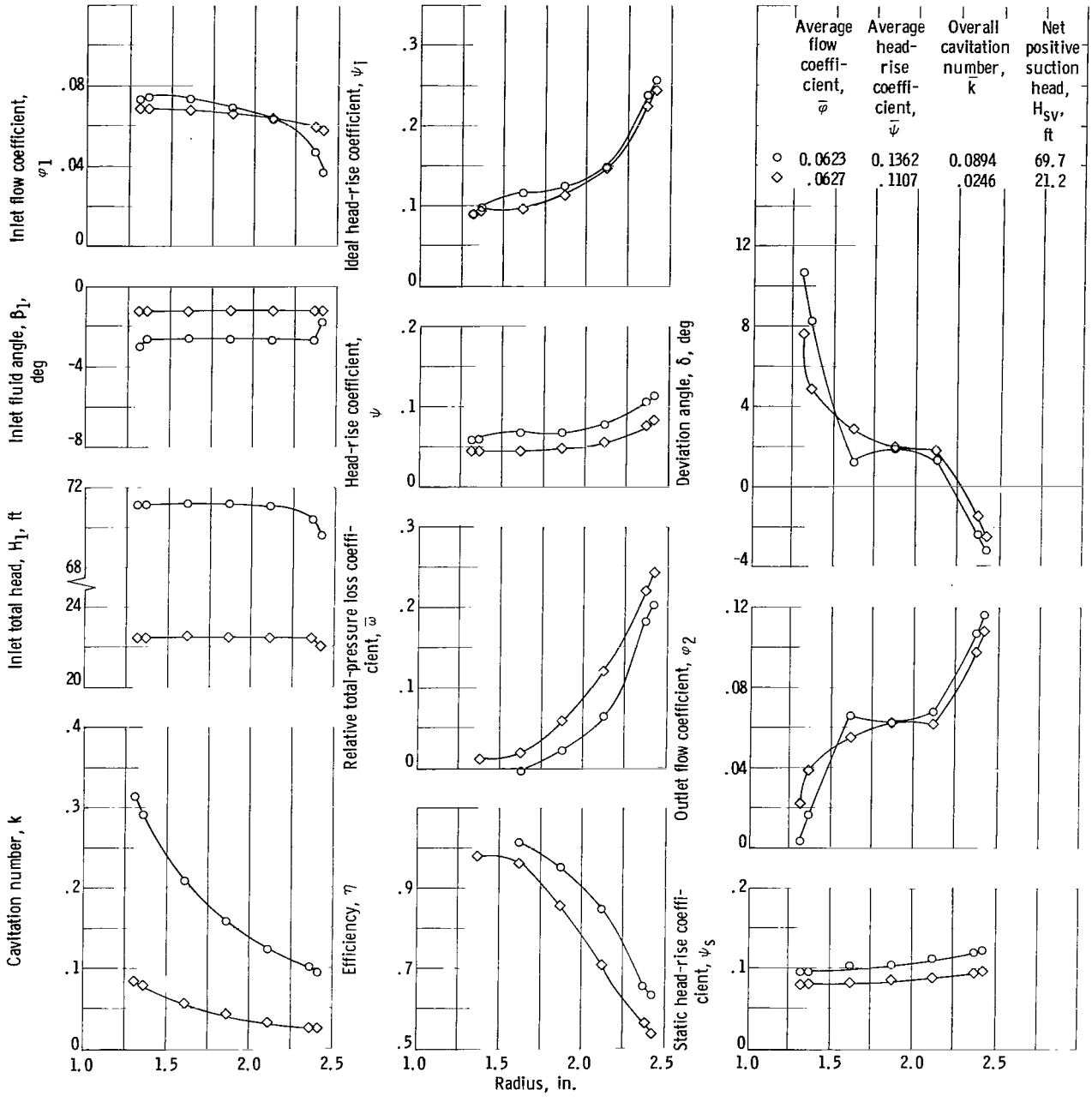

(d) Average flow coefficient, 0.0625.

Figure 14. - Concluded. Radial distribution of performance parameters.

As inlet pressure is reduced, the degree of cavitation increases so that the inducer can no longer maintain an established level of head rise. As shown in figures 14(a) to (d), the reduction in head-rise coefficient occurs at all radii in a roughly proportionate amount. This latter observation also applies to the ideal head-rise coefficient and to the static head-rise coefficient. This decrease in ideal head rise, which is a measure of energy addition, is one cause of the decrease in head rise.

The reduced values of ideal head rise appear to be due to the generally higher deviation angles observed under cavitating conditions as compared with noncavitating conditions. It should be pointed out, however, that cavitation blockage could give the same effects. Cavitation occurring at the blade trailing edge but collapsing before the outlet measuring station would give the same measured results as an increase in the actual deviation angle (defined as the deviation angle existing at the blade trailing edge). Both cavitation blockage and increased deviation angles would produce a decreased ideal head rise and an increased measured deviation angle (the deviation angle computed from outlet probe measurements). The two possibilities cannot be distinguished from the measured data.

The effects of cavitation on loss coefficient do not always show consistent trends; however, the general effect is for loss coefficient to increase as the degree of cavitation increases. Both lower energy addition and increased loss combine to give lower efficiencies.

The effects of cavitation on energy addition have been noted previously. Since the energy addition is reflected at a given radius in the outlet tangential velocity $V_{\theta,2}$, reduced values of $V_{\theta,2}$ result in decreases in the redistributions of axial velocity necessary to satisfy radial equilibrium. This effect is illustrated in figures 14(c) and (d). One result is that the average inlet-flow coefficient at which an eddy forms in the hub region at the blade outlet is lower for cavitating conditions than for noncavitating conditions. Also, the decrease in the radial gradient of energy addition tends to reduce the dropoff in flow coefficient at the inlet tip. The latter effects may be noted on the inlet distributions shown in figure 14(d).

Radial Equilibrium

The following equation, commonly called the simple-radial-equilibrium equation, is often used in design and analysis systems to describe the flow at the pump outlet:

$$\frac{\partial h}{\partial r} = \frac{V_{\theta,2}^2}{gr} \tag{3}$$

Figure 15 compares the measured outlet axial-velocity distribution with that computed from the simple-radial-equilibrium equation by using experimentally determined values of total pressure and fluid angle and by requiring the resulting flow distribution to give the outlet integrated mass-flow rate. The close agreement between the two indicates that most of the mass-flow shift takes place upstream of the outlet measuring station and establishes the validity of the simple-radial-equilibrium assumption at this axial location for all operating conditions.

To establish a design program requires, in addition to some expression of radial equilibrium, some method for prescribing the losses and deviation angles. As has been shown, mass-flow shifts and secondary flows strongly affect the values of loss coefficient and deviation angle in the helical inducer. (Radial flows would tend to make the indicated deviation angles vary with the axial

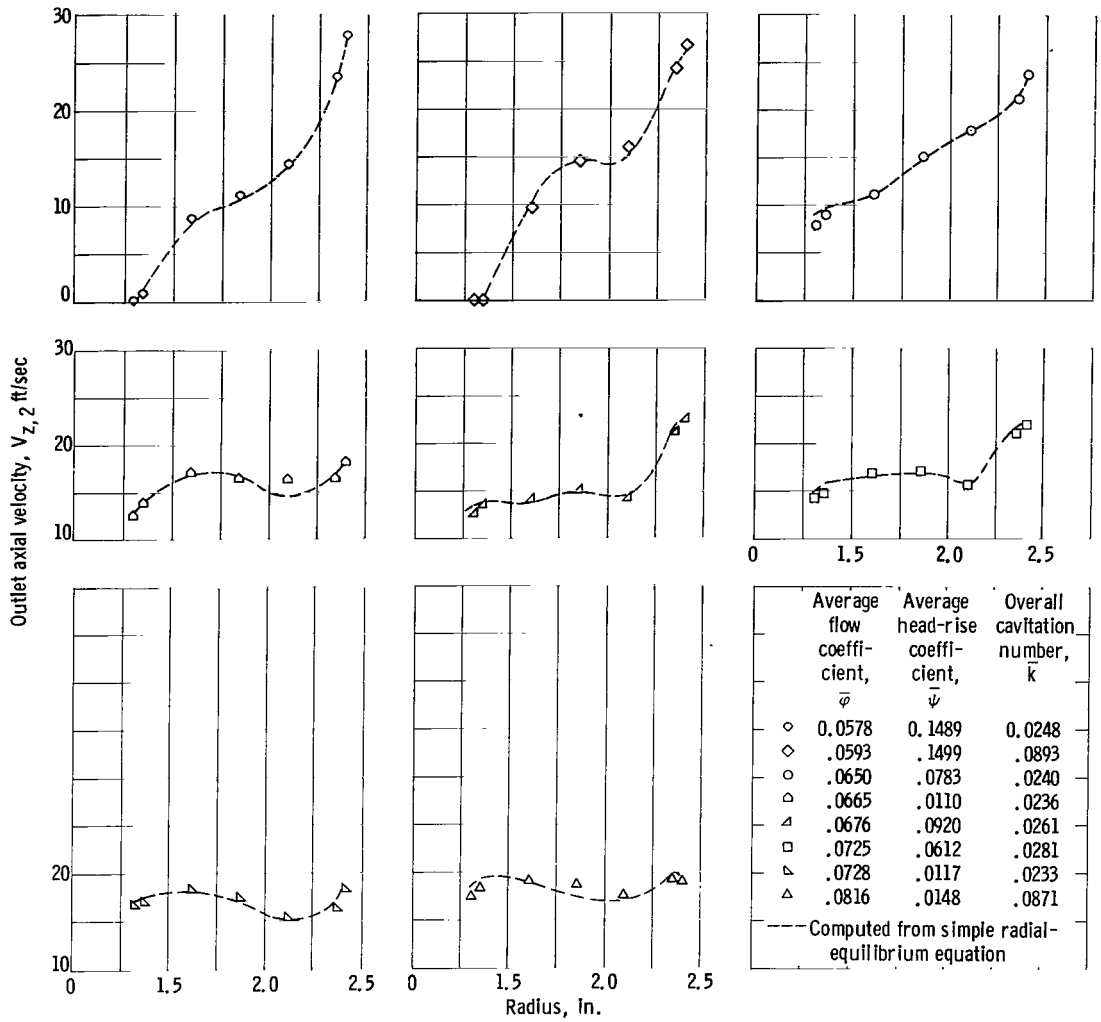

Figure 15. - Comparison of measured outlet axial velocity with axial velocity computed by simple radial-equilibrium equation.

location of the outlet probes; closer to the rotor, higher deviation angles would probably be measured.) A better understanding of these phenomena is required to allow a proper prescription of the parameters $\bar{\omega}$ and δ.

Comparison of Helical Inducer Performance at Three Blade Angles

Throughout this report considerable reference has been made to the similarities in performance trends of the subject inducer with those of references 1 and 2. The following discussion further compares the performance of the three inducers. Principal geometric features of the three inducers are summarized in table III. Throughout the three investigations, the same test facility, procedures, and measuring techniques were employed.

The overall performance under both cavitating and noncavitating conditions covered by the three investigations is presented in figure 16. While the data

TABLE III. - COMPARISON OF THREE HELICAL INDUCERS

	Blade tip angle, deg		
	78.0	80.6	84
Tip diameter, in.	4.956	4.956	4.986
Hub diameter, in.	2.478	2.478	2.478
Number of blades	3	3	3
Axial length, in.	2	2	1.637
Peripheral extent of blades, deg	215	280	360
Tip clearance, in.	0.030	0.030	0.025
Blade blockage ratio, volume occupied by blades/total passage volume	0.1312	0.1463	0.1512
Tip solidity	1.834	2.366	3.017
Hub solidity	1.937	2.447	3.060

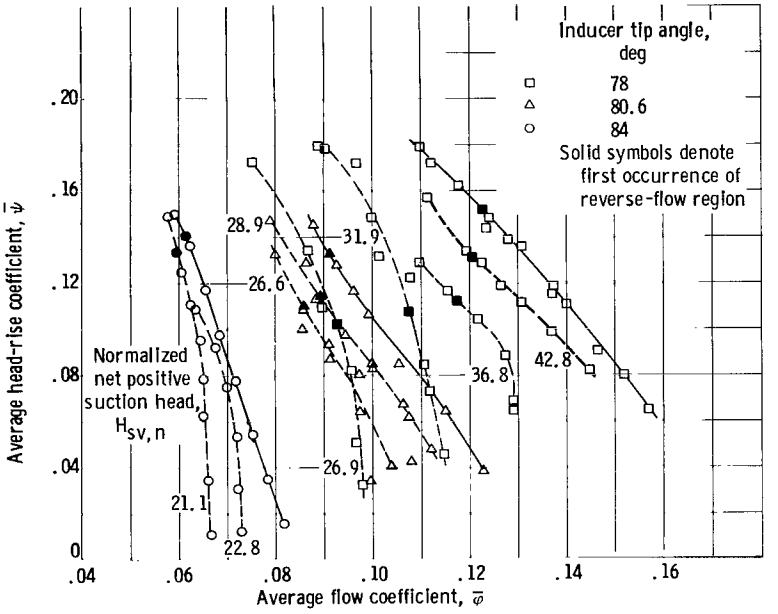

Figure 16. - Comparison of overall performance at three helix angles.

presented herein were obtained over a range of rotor speeds from 9000 to 15,000 revolutions per minute, the actual H_{sv} values were normalized to a speed of 10,000 revolutions per minute according to the relation

$$H_{sv,n} = H_{sv}\left(\frac{10,000}{N}\right)^2 \qquad (4)$$

The solid symbols on the performance curves for each individual inducer locate the operating conditions at which zero axial velocities are first observed at the hub outlet measuring station and thus denote the initial formation of an eddy, or reverse-flow region. If operation is continued to flow coefficients below this condition, the radial height of the eddy increases, along with noise and rig vibrations. Operation was discontinued when these vibrations threatened to become excessive, but no special criterion was used to determine a stall or surge point precisely.

In figure 17, cavitation performance of the three inducers is further compared by plotting the variation in head rise (normalized by the noncavitating value) against cavitation number for a constant flow coefficient. For the comparison, a flow coefficient for each inducer was selected that gave the best cavitation performance without giving a reverse-flow region at the hub under noncavitating conditions. The symbols represent data points at, or close to, the selected flow coefficients. As the incipient cavitation region is not defined by the data, no special significance should be attached to the manner in which the curves are faired into the noncavitating performance level.

Comparisons of cavitation performance are generally made at some selected percentage decrease from the noncavitating performance level. For a complete pump-inducer combination a dropoff in head rise from the noncavitating level of

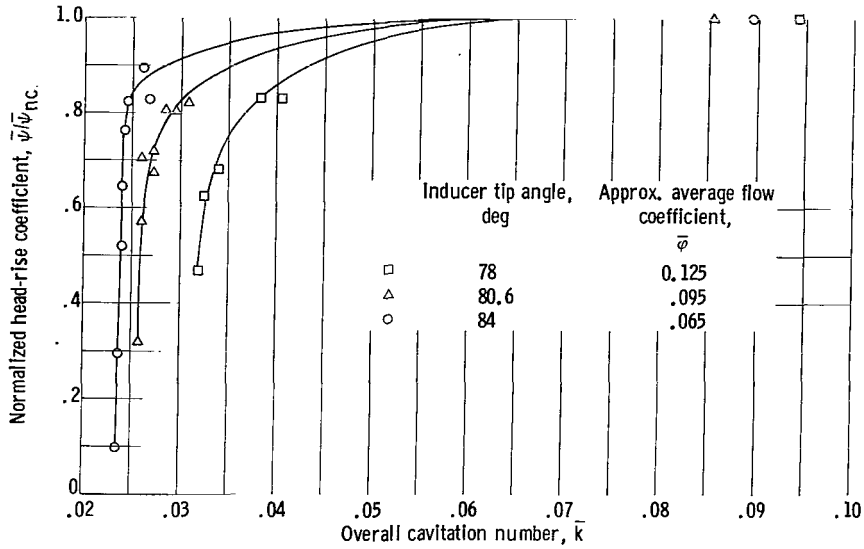

Figure 17. - Comparison of cavitation performance.

from 2 to 5 percent is generally used. For this degree of performance decrease in the complete pump, the percentage decrease in head rise across the inducer alone is generally much greater. Accordingly, the cavitating inducer data were primarily taken at head dropoffs of 15 percent or more.

For this region of head-rise dropoff, lower cavitation numbers were obtained at the higher helix angles; however, this does not necessarily produce higher suction specific speeds. In figure 18, the data points of figure 17 are replotted by using the suction-specific-speed parameter instead of $\bar{k}$. The 84° inducer has the highest S values only at the smaller head dropoffs, while below this the 80.6° inducer has a higher suction specific speed. The reason for this contrast can be explained if the analysis of references 4 and 5 is used. The relation between cavitation number, flow coefficient, and suction specific speed is given by

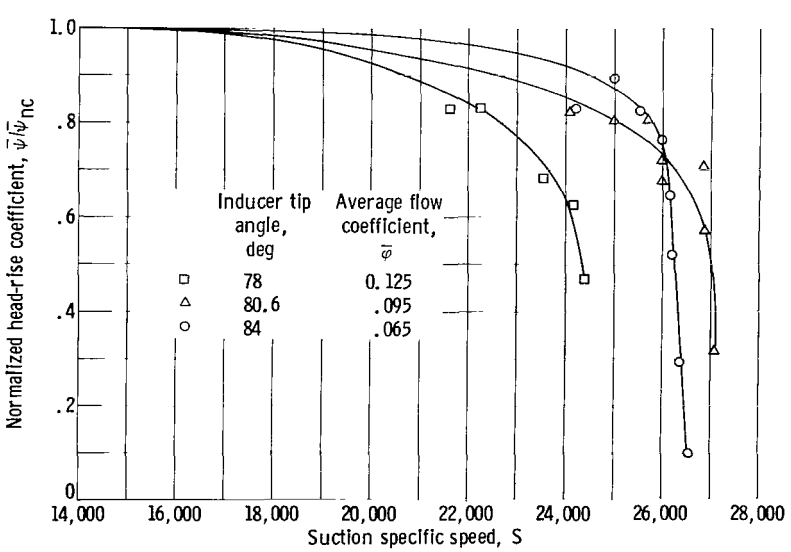

Figure 18. - Comparison of suction specific speeds.

$$S = \frac{8150\,\bar{\varphi}^{1/2}\sqrt{1 - \left(r_h/r_t\right)^2}}{\left[\bar{k}\left(1 + \bar{\varphi}^2\right) + \bar{\varphi}^2\right]^{3/4}} \qquad (5)$$

From the form of this equation it can be seen that of the two variables $\bar{\varphi}$ and $\bar{k}$, which both vary as blade angle is changed, a change in $\bar{k}$ has a

stronger effect on S; however, the effect of $\bar{\varphi}$ must also be considered. If $\bar{\varphi}$ is varied for a given constant value of $\bar{k}$, the suction specific speed will have a maximum value at an optimum value of average flow coefficient

$$\bar{\varphi}_{opt} = \sqrt{\frac{\bar{k}}{2(\bar{k} + 1)}} \tag{6}$$

and smaller values at both larger and smaller values of average flow coefficient. For the three inducers tested, the values of $\bar{\varphi}$ were less than $\bar{\varphi}_{opt}$, so that decreasing $\bar{\varphi}$ would tend to decrease S.

In general, as the blade angle of an inducer is increased, both $\bar{\varphi}$ and $\bar{k}$ will decrease. The usual result is an increase in S, as the effect of $\bar{k}$ is usually stronger than the effect of $\bar{\varphi}$. For the 84° inducer as compared with the 80.6° inducer, however, the decrease in $\bar{k}$ is relatively small, so that the effect of $\bar{\varphi}$ was enough to overshadow the usually stronger effect of $\bar{k}$.

It should be pointed out that much higher suction specific speeds are possible at a blade angle of 84°. From equation (6) it can be seen that decreasing $\bar{k}$ will also decrease φ_{opt}. Thus, any decrease in $\bar{k}$ will, in addition to the direct effect of increasing S, tend to alleviate the deleterious effects of the low $\bar{\varphi}$ value.

It appears from these data that, if suction specific speed is to continue to improve as flow coefficients fall below a value of approximately 0.10, blade designs leading to lower operating $\bar{k}$ values must be employed. (This fact is also indicated by the analysis of ref. 4.) Lower $\bar{k}$ values may be obtained by cutting back the leading edge of the blade or by making the blade thinner, particularly at the leading edge (ref. 6). Improved control of chordwise and spanwise loading distributions may require further study. In addition, better understanding of the secondary flow field and improved methods of calculating flow conditions and extent of cavities formed in blade channels may allow improved predictions of attainable suction performance in inducers.

SUMMARY OF RESULTS

The performance of a three-bladed flat-plate helical inducer with an 84° tip angle, a 5-inch diameter, and a hub-tip ratio of 0.5 was investigated. When a comparison is made with geometrically similar inducers with tip angles of 78° and 80.6°, the same trends are observed in all three inducers, so that the following statements may, unless otherwise stated, be generally applied to flat-plate inducers of this configuration:

For noncavitating conditions

1. For the 84° inducer, the maximum overall efficiency of 82.6 percent occurred at the lowest average flow coefficient obtained, 0.059.

2. There was an increase from hub to tip in the values of the blade-

element head-rise coefficient and in the related parameters, ideal head-rise coefficient and static head-rise coefficient. The radial gradients in these parameters increased as the flow was decreased.

3. As flow was reduced, radial equilibrium requirements at the blade exit resulted in the formation of an eddy in the hub region (indicated by zero axial velocity measurements). A further reduction in flow resulted in an eddy formation in the blade inlet tip region plus an increase in noise and rig vibrations.

4. A sharp increase in loss coefficient from the mean to the tip occurred for all operating conditions, indicating that the losses associated with secondary flows probably predominated over the profile losses.

For cavitating conditions

5. For the 84° inducer, cavitation breakdown occurred at an overall cavitation number $\bar{k}$ of 0.024 and a suction specific speed of approximately 26,000.

6. In general, cavitation decreased the head-rise-producing capability of the rotor (as indicated by the ideal head-rise coefficient) and increased both the loss level and the measured deviation angles.

7. The percentage decrease of head-rise coefficient, ideal head-rise coefficient, and static head-rise coefficient from the noncavitating value was approximately the same at all radii.

8. Cavitation tended to reduce or to eliminate entirely the eddies existing at the rotor inlet tip and outlet hub at the same flow coefficient under noncavitating conditions, a result of the decreased energy addition.

9. Under all flow conditions, both cavitating and noncavitating, the close correlation of the radial distribution of the measured axial velocities with those computed when simple radial equilibrium was assumed indicated the validity of this assumption.

A comparison of the performance of three similar helical inducers with rotor-tip helix angles of 78°, 80.6°, and 84° indicated

10. A given percentage performance dropoff from the noncavitating value occurred at lower overall cavitation numbers as the helix angle was increased.

11. The 84° inducer did not show the anticipated improvement in suction specific speed over the 80.6° inducer. At the overall cavitation numbers obtained, lowering average flow coefficient had an adverse effect on suction specific speed, which counteracted the effect of the lower cavitation numbers. At lower cavitation numbers this adverse effect would not occur, so that much better suction specific speeds are obtainable with the 84° inducer. It

appears that the operating cavitation number becomes critical below flow coefficients of about 0.10.

Lewis Research Center
National Aeronautics and Space Administration
Cleveland, Ohio, September 29, 1964

APPENDIX A

SYMBOLS

g	acceleration due to gravity, 32.17 ft/sec^2
H	total head, ft
ΔH	head rise across inducer, ft
H_{sv}	net positive suction head, ft (eq. (B1))
h	static head, ft
h_v	vapor pressure, ft
k	cavitation number (eq. (B10))
N	rotative speed, rpm
Q	flow rate, gal/min
r	radius, ft
S	suction specific speed (eq. (B11))
U	rotor speed, ft/sec
V	fluid velocity, ft/sec
β	fluid angle, angle between fluid velocity and axial direction, deg
γ	blade angle, angle between tangent to blade mean camber line and axial direction, deg
δ	deviation angle, deg
η	efficiency (hydraulic)
φ	flow coefficient
ψ	head-rise coefficient
$\bar{\omega}$	relative total-pressure loss coefficient

Subscripts:

h	hub
i	ideal

n normalized

nc noncavitating

opt optimum

s static pressure

t tip

v vapor pressure, or measured by Venturi meter

z axial direction

θ tangential direction

1 measuring station at rotor inlet

2 measuring station at rotor exit

Superscripts:

$-$ average or overall value except for loss coefficient $\bar{\omega}$

' relative to rotor

APPENDIX B

EQUATIONS FOR PERFORMANCE PARAMETERS

Blade-Element Calculations

Net positive suction head

$$H_{sv} = H_1 - h_v \tag{B1}$$

Ideal head rise

$$\Delta H_i = \frac{U_2 V_{\theta,2} - U_1 V_{\theta,1}}{g}$$

$$= \frac{U_2 V_{\theta,2}}{g} \quad (V_{\theta,1} = 0) \tag{B2}$$

Head-rise coefficient

$$\psi = \frac{g\,\Delta H}{U_t^2} \tag{B3}$$

Ideal head-rise coefficient

$$\psi_i = \frac{g\,\Delta H_i}{U_t^2} \tag{B4}$$

Static head-rise coefficient

$$\psi_s = \frac{g(h_2 - h_1)}{U_t^2} \tag{B5}$$

Flow coefficient

$$\varphi = \frac{V_z}{U_t} \tag{B6}$$

Relative total pressure-loss coefficient

$$\overline{\omega} = \frac{H'_{2,i} - H'_2}{V_1'^2/2g} = \frac{\Delta H_i - \Delta H}{V_1'^2/2g} \tag{B7}$$

Deviation angle

$$\delta = \beta' - \gamma_2 \tag{B8}$$

Efficiency (hydraulic)

$$\eta = \frac{\Delta H}{\Delta H_i} = \frac{\Delta H}{(U_2 V_{\theta,2} - U_1 V_{\theta,1})/g} \tag{B9}$$

Cavitation number

$$k = \frac{h_1 - h_v}{V_1^{i2}/2g} \tag{B10}$$

Suction specific speed

$$S = \frac{N\sqrt{Q}}{(H_{sv})^{3/4}} \tag{B11}$$

Overall Performance Calculations

Average flow coefficient

$$\overline{\varphi} = \frac{\overline{V}_z}{\overline{U}_t} \tag{B12}$$

Average axial velocity

$$\overline{V}_z = \frac{Q_v}{448.8\ \pi\left(r_t^2 - r_h^2\right)} \tag{B13}$$

Integrated flow rate

$$\left.\begin{aligned} Q_1 &= 448.8 \int_{r_h}^{r_t} 2\pi V_{z,1} r\ dr \\ Q_2 &= 448.8 \int_{r_h}^{r_t} 2\pi V_{z,2} r\ dr \end{aligned}\right\} \tag{B14}$$

Mass-averaged inlet total head

$$\bar{H}_1 = \frac{\int_{r_h}^{r_t} V_{z,1} r_1 H_1 \, dr_1}{\int_{r_h}^{r_t} V_{z,1} r_1 \, dr_1} \tag{B15}$$

Mass-averaged outlet total head

$$\bar{H}_2 = \frac{\int_{r_h}^{r_t} V_{z,2} r_2 H_2 \, dr_2}{\int_{r_h}^{r_t} V_{z,2} r_2 \, dr_2} \tag{B16}$$

Mass-averaged head-rise coefficient

$$\bar{\psi} = \frac{g}{U_t^2} (\bar{H}_2 - \bar{H}_1) \tag{B17}$$

Mass-averaged efficiency

$$\bar{\eta} = \frac{\int_{r_h}^{r_t} V_{z,2} r_2 \eta \, dr_2}{\int_{r_h}^{r_t} V_{z,2} r_2 \, dr_2} \tag{B18}$$

Overall cavitation number

$$\bar{k} = \frac{2gH_{sv}}{U_t^2(1 + \bar{\varphi}^2)} - \frac{\bar{\varphi}^2}{1 + \bar{\varphi}^2} \tag{B19}$$

Normalized net positive suction head

$$H_{sv,n} = H_{sv}\left(\frac{10,000}{N}\right)^2 \tag{B20}$$

REFERENCES

1. Soltis, Richard F., Anderson, Douglas A., and Sandercock, Donald M.: Investigation of the Performance of a 78° Flat-Plate Helical Inducer. NASA TN D-1170, 1962.

2. Sandercock, Donald M., Soltis, Richard F., and Anderson, Douglas A.: Cavitation and Noncavitation Performance of an 80.6° Flat-Plate Helical Inducer at Three Rotational Speeds. NASA TN D-1439, 1962.

3. Montgomery, John C.: Analytical Performance Characteristics and Outlet Flow Conditions of Constant and Variable Lead Helical Inducers for Cryogenic Pumps. NASA TN D-583, 1961.

4. Huppert, M. C., King, W. S., and Stripling, L. B.: Some Cavitation Problems in Rocket Propellant Pumps. Rocketdyne, North Am. Aviation, Inc., 1960.

5. Ross, C. C., and Banerian, Gordon: Some Aspects of High Suction-Specific-Speed Pump Inducers. Trans. ASME, vol. 78, no. 8, Nov. 1956, pp. 1715-1721.

6. Stripling, L. B.: Cavitation in Turbopumps, pt 2. Paper 61-WA-98, ASME, 1961.

2/11/65

"The aeronautical and space activities of the United States shall be conducted so as to contribute . . . to the expansion of human knowledge of phenomena in the atmosphere and space. The Administration shall provide for the widest practicable and appropriate dissemination of information concerning its activities and the results thereof."

—NATIONAL AERONAUTICS AND SPACE ACT OF 1958

NASA SCIENTIFIC AND TECHNICAL PUBLICATIONS

TECHNICAL REPORTS: Scientific and technical information considered important, complete, and a lasting contribution to existing knowledge.

TECHNICAL NOTES: Information less broad in scope but nevertheless of importance as a contribution to existing knowledge.

TECHNICAL MEMORANDUMS: Information receiving limited distribution because of preliminary data, security classification, or other reasons.

CONTRACTOR REPORTS: Technical information generated in connection with a NASA contract or grant and released under NASA auspices.

TECHNICAL TRANSLATIONS: Information published in a foreign language considered to merit NASA distribution in English.

TECHNICAL REPRINTS: Information derived from NASA activities and initially published in the form of journal articles.

SPECIAL PUBLICATIONS: Information derived from or of value to NASA activities but not necessarily reporting the results of individual NASA-programmed scientific efforts. Publications include conference proceedings, monographs, data compilations, handbooks, sourcebooks, and special bibliographies.

Details on the availability of these publications may be obtained from:

SCIENTIFIC AND TECHNICAL INFORMATION DIVISION

NATIONAL AERONAUTICS AND SPACE ADMINISTRATION

Washington, D.C. 20546